Ground-state properties of multivalent manganese oxides: Density functional and hybrid density functional calculations

C. Franchini* and R. Podloucky
Department of Physical Chemistry, University of Vienna and Center for Computational Materials Science, Sensengasse 8, A-1090 Vienna, Austria

J. Paier, M. Marsman, and G. Kresse
Department of Materials Physics, University of Vienna and Center for Computational Materials Science, Sensengasse 8, A-1090 Wien, Austria

(Received 6 February 2007; revised manuscript received 7 March 2007; published 25 May 2007)

We present density functional theory (DFT) calculations for MnO, Mn_3O_4, α-Mn_2O_3, and β-MnO_2, using different gradient corrected functionals, such as Perdew-Burke-Ernzerhof (PBE), PBE+U, and the two hybrid density functional Hartree-Fock methods PBE0 and Heyd-Scuseria-Ernzerhof (HSE). We investigate the structural, electronic, magnetic, and thermodynamical properties of the mentioned compounds. Despite the lack of sufficient experimental information allowing for a comprehensive comparison of our results, we find overall that hybrid functionals provide a more consistent picture than standard PBE. Although PBE+U is limited due to the uncertainty of choosing the parameter U, it nevertheless provides satisfactory results in terms of magnetic properties and energies of formation. This is in line with results of PBE0 and HSE calculations, but the PBE+U approach tends to overestimate the equilibrium volumes, and also it favors a half-metallic state for the more reduced oxides Mn_3O_4, α-Mn_2O_3, and β-MnO_2, rather than an insulating character as derived from the hybrid functional approaches. The comparison of measured valence-band spectra with the HSE density of states offers a further assessment of the capability of hybrid approaches in overcoming the deficiencies of DFT in treating these kinds of materials.

DOI: 10.1103/PhysRevB.75.195128 PACS number(s): 71.27.+a, 71.15.Mb, 71.15.Nc, 77.84.Bw

I. INTRODUCTION

Manganese oxides have been exploited since ancient times for pigments and for purifying glass. Nowadays, they are widely used in catalytic processes and in alkaline and dry-cell batteries. Other applications include production of water-purifying agents, plant fertilizers, and pesticides.[1] From a fundamental point of view, manganese oxide materials have gained much attention because of the presumably rather strong electron correlation, which leads to interesting phenomena such as colossal magnetoresistance, orbital ordering, and exotic magnetic structures (helimagnetism, canted spins, etc.).[2–21]

Manganese oxides crystallize in a remarkable variety of structures within a wide range of multivalent phases, which are related to the three different oxidation states of manganese of +2, +3, and +4. In the present work, we focus our attention on MnO, Mn_3O_4, α-Mn_2O_3, and β-MnO_2. MnO is a type-II antiferromagnetic insulator[2,3] and crystallizes in a rhombohedrally distorted B1 structure.[4] Its structural, electronic, and magnetic properties have been also widely studied by a number of different computational approaches, ranging from *GW*,[5] self-interaction corrections (SIC),[6] LSDA+U,[7] to hybrid functionals.[8,9] Mn_3O_4 possess a tetragonally distorted spinel structure and is characterized by a complex canted spin structure which has gained much attention both experimentally[11–13] and theoretically.[14] The magnetic and crystallographic properties of α-Mn_2O_3 has been investigated by Grant *et al.*[15] These authors report two antiferromagnetic (AFM) transitions at 80–90 K and 25 K and a cubic to orthorhombic structural transition at 308 K. However, the magnetic structure of α-Mn_2O_3 still remains under debate.[16,17] To our knowledge, no theoretical studies have been reported in the literature for this compound. Finally, despite its simple rutile-type structure, β-MnO_2 shows very intriguing magnetic[18] and transport properties.[19] According to Yoshimori,[20] below 92 K the spins are aligned following the so-called screw-type magnetic structure, which has also been investigated using a tight-binding approach by Zhuang *et al.*[21]

Though this class of materials has been extensively studied in past decades, a consistent and rigorous theoretical description of its ground-state properties within a computational framework, capable of correctly predicting the electronic structure for all three oxidation states, is still missing. Such a task presents a fundamental challenge for computational methods based on density functional theory (DFT).

It is well known that DFT within the standard local-density approximation (LDA) or generalized gradient approximation (GGA) to the exchange and correlation functional, experiences severe limitations in describing the physics of magnetic materials with strongly localized electronic states. This is due to the spurious, self-interaction (SI) of the localized electrons, which is only partially cancelled in the LDA and GGA approximations and which induces a wrong treatment of the Coulomb interaction.[22] Many different methods have been proposed to overcome this fundamental limitation of standard DFT approaches, varying from the rather popular DFT+U method[23] to the more sophisticated self-interaction corrections[24] (SIC) and Green's-function-based[25] (*GW*) approaches. More recently, a

class of functionals incorporating a fraction of the Hartree-Fock (HF) exchange has been proposed, the so-called hybrid functionals,[26] which have been successfully applied to a wide class of systems.[27–31]

The spurious SI strongly depends on the nature of electronic orbitals and is particularly large for localized states, such as the Mn *d* states in MnO, in which Mn occurs in a +2 state. MnO is indeed the prototype of an intermediate Mott-Hubbard/charge-transfer insulator (i.e., the top of the valence band is of mixed O $2p$-Mn e_g character) with a rather large insulting gap of ≈4 eV. For compounds with higher oxidation states of Mn, the interplay of correlation, magnetic, and structural effects reduces the insulating character, which finally is nearly suppressed for MnO_2.[19]

An additional obstacle for any *ab initio* calculations is the prediction of the heats of formation of molecules and solids, in particular for oxides of 3*d* transition metals.[32] Since redox reactions play a prominent role in many technological processes, the ability to calculate reliable oxidation energies using *first-principles* techniques is of significant importance. Very recently, Wang *et al.*[32] have shown that GGA suffers from systematic errors in evaluating the energy of oxidation reactions. These authors found that these drawbacks can be corrected using the GGA+U approach and by applying an *ad hoc* change of the O_2 reference energy.[22] Despite its improved performance, the above method has the fundamental limitation of choosing the on-site Coulomb repulsion parameter U, which is usually chosen to maximize the agreement with some experimental quantity. Such a procedure is rather unsatisfactory for an *ab initio* methodology. Furthermore, the value of U might be very different for oxides containing transition metal atoms in different oxidation states. Because total energies calculated using different values of U cannot be compared, one single value of U must be chosen for all phases in order to encompass a set of energies of different multivalent oxides within a common DFT+U formalism. As a matter of fact, a single U correctly accounting for the solid state properties of, for example, MnO and MnO_2 cannot be found. Therefore, the use of DFT+U in calculating heats of formation and other ground-state properties for a given class of metal oxides suffers from the unavoidable compromise in the choice of U.

In summary, to establish a computational approach able to deal with the wide range of manganese oxidation states within a single coherent framework is highly desirable. To this end, hybrid functionals might provide an improved picture thanks to the way in which nonlocal exchange and correlation effects are incorporated. In contrast to DFT+U, which operates essentially only on localized states, the orbital dependent character of the hybrid functionals allows for an automatic treatment of exchange and correlation effects in both extended as well as localized states. To some extent, hybrid DFT would also require a material dependent amount of Fock exchange.[29,31] It should be emphasized, however, that the optimized choice of one unique parameter entering the PBE0-type hybrid functional[33] was found to reproduce well the magnetic and electronic properties of a wide class of systems.[30,33]

The aim of the present work is to investigate the ground-state properties (structural properties, electronic character, magnetic ordering, and oxidation energies) of four oxides that contain manganese in the +2, +3, and +4 states, namely MnO, Mn_3O_4, α-Mn_2O_3, and β-MnO_2, using standard GGA and GGA+U methods as well as hybrid Hartree-Fock DFT approaches. We will show that, though the hybrid functional approach faces significant obstacles in describing the physics of metallic/quasimetallic materials, it is found to be the most adequate technique for studying multivalent manganese oxides.

The paper is organized as follows. In Sec. II we describe the computational tools. In Sec. III and corresponding subsections we present the results. Finally, in Sec. IV we draw conclusions.

II. COMPUTATIONAL ASPECTS

All calculations have been performed using the projector-augmented-wave (PAW) based[34,35] *Vienna ab initio Simulation Package* (VASP).[36,37] Four different approximations to treat exchange and correlation have been applied: (i) the PBE approach utilizing a standard GGA scheme according to the parameterization of Ref. 38, (ii) the PBE+U method following the approach of Dudarev[39] for three values for U-J (namely 6, 4, and 3 eV), and the two types of hybrid functionals, (iii) the PBE0 approach,[33,40] and (iv) the HSE method,[41,42] as implemented in VASP.[43,44] The PBE0 and HSE approaches have in common that they mix 25% of the exact HF exchange with 75% of the PBE exchange functional. The difference of these two methods is in the treatment of the long-range part of exact exchange interaction. In the HSE functional, only the the short-range component is preserved in the nonlocal part. The cutoff of the long-range part allows us to overcome the convergence problem associated with the slow decay of the Coulomb $\frac{1}{r}$ kernel. The screening parameter ω was chosen to be 0.3 $Å^{-1}$ for the nonlocal and local part as originally suggested by Heyd, Scuseria, and Ernzerhof.[41] We note that this is not identical to the implementation of the HSE03 functional in the Gaussian suite (see Erratum in Ref. 45).

By calculating the stress tensor, forces, and total energies, the unit cell shapes, volumes, and internal structural parameters were optimized for all crystal structures considered. A cutoff of 400 eV was chosen for the plane-wave basis set. The Monkhorst and Pack type $\vec{k}$-point grid[46] was optimized for each structure, in order to achieve an optimal compromise between accuracy and computing time. A $4\times4\times4$ grid was chosen for the least demanding cases of MnO and β-MnO_2, whose unit cells contain only four and six atoms, respectively. For Mn_3O_4, with 16 atoms per unit cell, a $2\times2\times2$ grid was applied, whereas for the complex crystal structure of α-Mn_2O_3, with 80 atoms per unit cell, only the Γ point was chosen. The relations, by which the energies of formation are calculated, are discussed in Sec. III D.

III. RESULTS

Table I lists some basic properties of the compounds investigated, including the oxidation states, crystal structural data and observed magnetic orderings. A sketch of the four

TABLE I. Properties of manganese oxides under study: Mn concentration, oxidation state, space group symmetry, and magnetic ordering.

	% Mn	State	Oxidation Space Group Symmetry	Magnetic Ordering
MnO	50	+2	$Fm3m$	AFM-II
Mn_3O_4	43	+2, +3	$I4_1/amd$	Ferrimagnetic
α-Mn_2O_3	40	+3	$Pcab$	Noncollinear
β-MnO_2	33	+4	$P4_2/mnm$	Helical

different lattices is depicted in Fig. 1. A more detailed discussion of the ground-state properties is given in the appropriate subsections. At this point we want to mention that we simulated the nontrivial magnetic arrangements of Mn_3O_4, α-Mn_2O_3, and β-MnO_2 by collinear ferromagnetic (FM), antiferromagnetic (AFM), and ferrimagnetic (FiM) orderings of the local magnetic moments. In the following, only the results for the most stable magnetic arrangements will be discussed.

A. Structural properties

We will discuss the structural properties in terms of the equilibrium volumes as calculated by minimizing the stress tensor and total energies. Although a full minimization of the internal structural degrees of freedom was also performed (which is required for an accurate description of the electronic and magnetic structure), a detailed presentation of the atomic positions and internal distortions as a function of the computational method is beyond the purposes of the present study, and therefore it will be described elsewhere.

The calculated volumes together with experimental data are shown in Table II and sketched in Figure 2, in which the calculated volumes per atom are compared to experimental findings. As mentioned above, α-Mn_2O_3 has the computationally most demanding structure. To save computing time, the structure of α-Mn_2O_3 was not optimized using the PBE0 functional, since it is generally found that the PBE0 and the HSE functionals yield structural parameters within a few fractions of a percent. The energy and electronic properties of α-Mn_2O_3 were calculated using the structure optimized using the HSE functional.

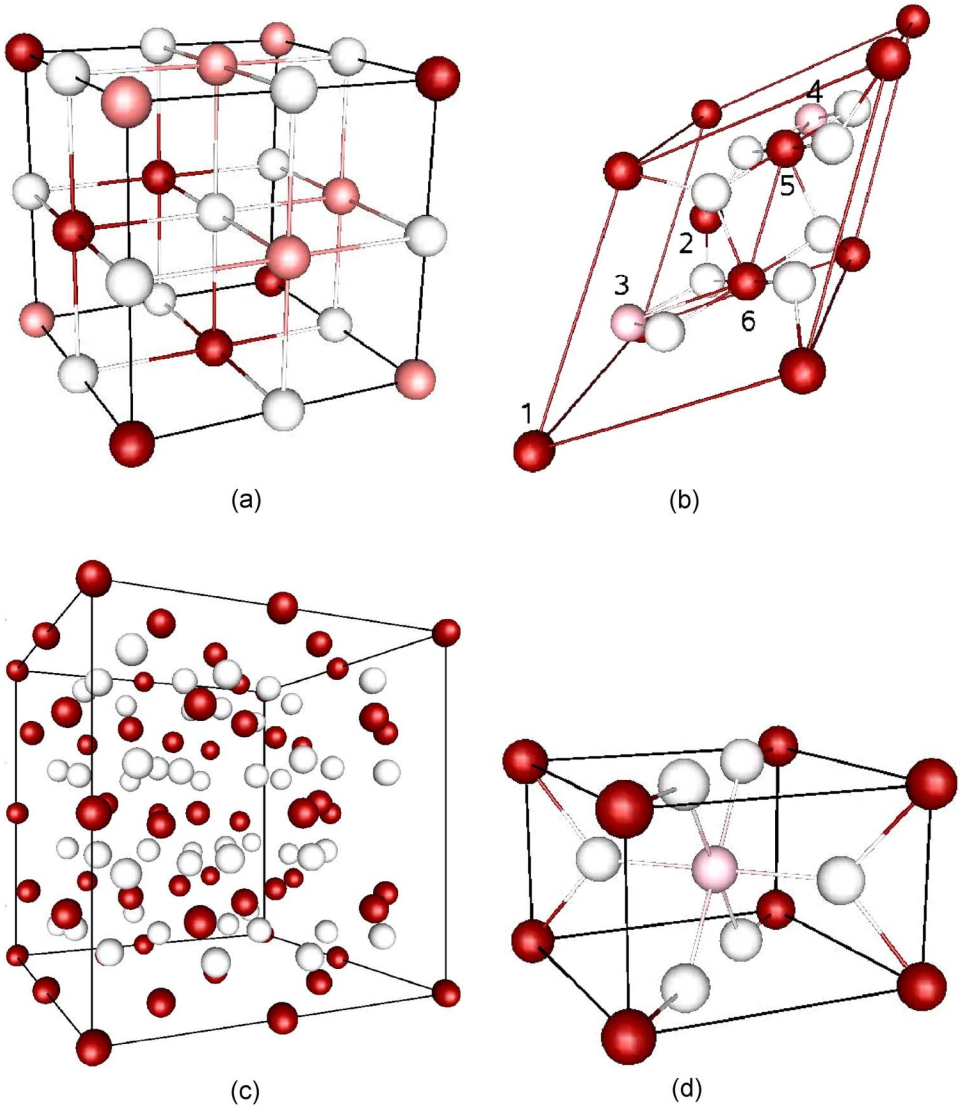

FIG. 1. (Color online) Schematic ball and stick representation of (a) MnO, (b) Mn_3O_4, (c) α-Mn_2O_3, and (d) β-MnO_2. White spheres indicate oxygen atoms whereas black (red) and gray (pink) balls indicate spin-up and spin-down Mn atoms, respectively. Magnetic ordering corresponds to optimal HSE low-energy structure.

TABLE II. Equilibrium volumes V_0 (Å^3 per formula unit) as calculated by the PBE+U, PBE, PBE0, and HSE approaches. The PBE+U volumes refer to a set of three different calculations for sU=6 eV (PBEU6), U=4 eV (PBEU4), and U=3 eV (PBEU3). The comparison with experimental volumes is given in terms of the relative error (RE, in %), and its mean absolute relative value over the whole class of oxides (MARE).

	PBEU6	PBEU4	PBEU3	PBE	PBE0	HSE	Expt.
MnO	45.12	45.10	44.73	43.53	43.54	43.46	43.6[a]
	3.5	3.4	2.6	−0.2	−0.1	−0.3	
Mn_3O_4	166.31	164.20	162.93	158.33	157.42	156.01	155.73[b]
	6.8	5.4	4.6	1.7	1.1	0.2	
α-Mn_2O_3	900.57	882.90	875.65	836.86		845.83	834.48[c]
	7.9	5.8	4.9	0.3		1.4	
β-MnO_2	62.33	59.32	57.82	56.49	55.06	55.30	55.48[d]
	12.5	7.1	4.3	1.8	−0.7	−0.3	
MARE	7.7	5.4	4.1	1.0		0.6	

[a]Reference 47.
[b]Reference 48.
[c]Reference 49.
[d]Reference 50.

At first, we remark that GGA functionals generally overestimate the equilibrium volume, whereas the Hartree-Fock approximation yields volumes that are too small. Hybrid functionals, therefore, tend to give very good volumes within 1% of the experimental data. In Table II, we report, for each compound, the theoretical volume and the corresponding relative error (RE) with respect to the experimental data. In the last row, the average mean absolute relative error (MARE) estimated for each method by averaging over the four systems, supplies an indication of the global performance of the various approaches applied.

Table II reveals that the PBE+U method significantly overestimates the experimental volumes. This deviation appears to be strongly dependent on U and the system under study: (i) for increasing values of U the relative error increases, in line with the known tendency of PBE+U to overestimate bondlengths; (ii) the DFT+U method fails dramatically going towards the bottom of the table, namely for systems with progressively less localized Mn-3*d* electrons, for which DFT+U appears to be inadequate. In fact, as a rule of thumb, smaller self-interaction should correspond to a smaller value of U. The best structural description within the PBE+U method is achieved for U=3 eV. However, the relative error is still rather large ($\approx$4%) and—as discussed in the following sections—a rather small value of U=3 eV describes other physical quantities in a less satisfactory manner, which is particularly obvious for MnO as a strongly correlated system.

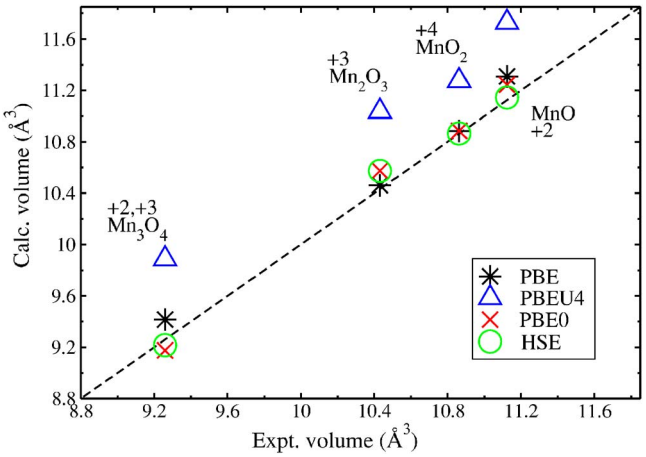

FIG. 2. (Color online) Comparison between calculated (by the PBE, PBE+U, PBE0, and HSE approaches) and experimental equilibrium volumes (Å^3/atom). The manganese oxidation states are also indicated.

A much better prediction of the volumes is achieved by, standard PBE and hybrid functionals, which give very small errors (RE within 1%), as clearly visualized by Fig. 2. The MARE is smaller for the hybrid functionals, although PBE outperforms the HSE functional for α-Mn_2O_3. Nonetheless, the improvement of PBE0 and HSE with respect to PBE goes beyond the structural properties, as discussed below. Apart from MnO, for which several theoretical investigations exist[5–9] (which are essentially in line with our findings), the only other theoretical work that can be compared to our data is the Hartree-Fock study of Chartier *et al.*[14] These authors reported a volume of 164.01 Å^3 for Mn_3O_4, which is 5% larger than the experimental one.

B. Magnetic properties

The magnetic properties of manganese oxides are particularly intriguing. Indeed, most of the attention addressed to this class of systems was on the understanding of their unusual magnetic orderings. Low-temperature magnetic measurements have shown that (i) MnO crystallizes in the antiferromagnetic type II (AFM-II) arrangement, (ii) Mn_3O_4 exhibits a noncollinear ferrimagnetic (NC-FiM) behavior below a commensurate-incommensurate transition temperature T_t=33 K, (iii) α-Mn_2O_3 displays a complex noncollinear

TABLE III. Calculated optimized magnetic orderings and local spin magnetic moments (μ_B) and available experimental data (last column). For more details, see text.

	PBEU6	PBEU4	PBEU3	PBE	PBE0	HSE	Expt.
MnO	AFM-II	AFM-II	AFM-II	AFM-II	AFM-II	AFM-II	AFM-II
	4.67	4.59	4.54	4.31	4.52	4.51	4.58[a]
							4.79[b]
Mn_3O_4	FiM3	FiM3	FiM3	FiM3	FiM3	FiM3	NC-FiM
	3.97–4.67	3.81–4.57	3.72–4.51	3.37–4.22	3.69–4.50	3.68–4.48	
α-Mn_2O_3	FM	FM	FM	AFM	FM	FM	NC-AFM
	4.24	4.07	3.97	2.47–3.72	3.80–3.84	3.81–3.84	3.4–3.9[c]
β-MnO_2	FM	FM	AFM	AFM	AFM	AFM	Helical
	3.34	3.28	2.93	2.51	2.89	2.89	1.84–2.35[c]

[a]Reference 51.
[b]Reference 52.
[c]Reference 17.

AFM ordering not yet unequivocally resolved, and finally (iv) β-MnO_2 has a screw-type magnetic structure with helically ordered moments, again not yet fully understood.

Within this scenario, the simulation of the experimentally observed magnetic configurations appears to be very complicated. In principle, our theoretical approach would allow for the treatment of noncollinear orderings. However, due to the computational cost required for this purpose, such calculations are presently very problematic within the PAW hybrid DFT framework as implemented in VASP, in particular for α-Mn_2O_3. Therefore, we only consider *idealized* collinear magnetic couplings, describing possible AFM/FM/FiM interactions compatible with the given crystalline unit supercell, as described below.

MnO was studied in its experimental AFM-II arrangement. Other magnetic orderings were found to be significantly less stable within both standard and hybrid DFT calculations. To account for the tetragonally distorted spinel structure of Mn_3O_4, we have employed a base centered monoclinic cell containing two formula units (f.u.) with 6 Mn atoms per unit cell [see Fig. 1(b)]. For this phase we have studied FM and six different FiM orderings, following the labeling of Chartier *et al.*[14] If the Mn atoms of the primitive cell are labeled 1 to 6 [see Fig. 1(b)], the magnetic orderings are indicated as FM=($\uparrow\uparrow\uparrow\uparrow\uparrow\uparrow$), FiM1 =($\downarrow\downarrow\uparrow\uparrow\uparrow\uparrow$), FiM2=($\uparrow\downarrow\uparrow\uparrow\uparrow\uparrow$), FiM3=($\uparrow\uparrow\downarrow\downarrow\uparrow\uparrow$), FiM4=($\uparrow\uparrow\uparrow\downarrow\uparrow\downarrow$), FiM5=($\uparrow\uparrow\uparrow\downarrow\uparrow\uparrow$), FiM6=($\uparrow\downarrow\uparrow\downarrow\uparrow\downarrow$). We found the FiM3 arrangement to be the most stable magnetic configuration.

The cubic unit cell of α-Mn_2O_3 houses 16 f.u. which amounts to 32 Mn atoms. The magnetic configurations of this system have been modeled with the FM coupling and three selected FiM spin arrangements. Finally, β-MnO_2 (with a unit cell comprising two f.u.) was studied for FM and AFM orderings. For all magnetic structures, geometrical parameters were fully optimized.

Table III summarizes our findings. For each structure and applied method the most stable magnetic configuration is indicated, along with the value of the calculated spin magnetic moment. For completeness, the last column lists the available experimental informations. For the reasons given above, a direct comparison with experiment might be speculative. We use Table III for discussing the relative performance of the various methods applied.

For MnO and Mn_3O_4, all approaches agree about the most stable magnetic configuration, AFM-II and FiM3, respectively. However, two important differences arise. The FiM phases are generally very close in energy, but for Mn_3O_4 the relative stability of the FiM3 phase with respect to the less favorable FiM2 configuration ranges from $\approx$200 meV/f.u. (PBE) to $\approx$70 meV (PBE+U and hybrid DFT). This difference significantly affects the value of the exchange coupling parameters, as discussed in Ref. 14. Second, remarkable deviations are observed for the values of the spin magnetic moment: the values for the hybrid DFT approximation are somewhere between the large PBE+U values and the smaller standard PBE results. This is a general feature common to all manganese oxides. In general, the hybrid functional results seem to agree best with experiment, although the experimental uncertainties render such a statement rather tentative.

The performance of the different theoretical methods is less uniform for α-Mn_2O_3 and β-MnO_2. Despite an experimentally observed NC-AFM phase, PBE+U and hybrid DFT find the FM configuration to be more stable by about 150 meV/f.u. than AFM-type orderings. However, HSE and PBE0 give a value for the spin magnetic moment in very good agreement with the experimental data. The increased magnetic moment for the hybrid functionals compared to PBE is most likely also responsible for the increased HSE volume (see Table II; magnetovolume effect). Finally, for β-MnO_2, all calculations prefer an AFM phase, apart from PBE+U which, for U=4 and 6, favors an FM coupling. For this system the predicted spin magnetic moments are found to be too large compared to the measured values.

C. Electronic structure

Apart from the case of MnO, which properties have been extensively investigated using a wide variety of methods,[5–9] the number of studies dealing with the electronic properties

TABLE IV. Results of DFT, DFT+U, and hybrid DFT calculations for the electronic gap (eV). The label HM refers to a half-metallic ground state, for which the gap corresponding to the insulating spin channel is given. For Mn_3O_4 and α-Mn_2O_3, we list both the minority and majority PBE0 and HSE gaps.

	PBEU6	PBEU4	PBEU3	PBE	PBE0	HSE	Expt.
MnO	2.1	1.8	1.6	0.9	3.8	2.9	3.6–4.2[a,b]
Mn_3O_4	0.5	0.4	0.3	0.0	2.4	1.7	
	HM	HM	HM		3.2	2.3	
α-Mn_2O_3	4.1	3.5	3.1	0.0	1.1	0.1	
	HM	HM	HM		5.8	4.0	
β-MnO_2	0.0	0.0	0.0	0.0	1.5	0.6	

[a]Reference 54.
[b]Reference 56.

of other manganese oxides is very scarce, concerning both experimental and theoretical efforts. This lack of information in combination with the difficulties that DFT encounters in treating this class of materials, aggravates the interpretation of our predictions for the electronic structure of the Mn_xO_y compounds. Nevertheless, in order to shed some light on this intricate subject, we supply a tentative summary of our results.

The insulating nature of MnO is well established. Experimental results for its insulating gap are in the range of 3.6 to 4.2 eV, and accurate *ab initio* studies characterize MnO as an intermediate Mott-Hubbard/charge-transfer compound. The situation is much less clear for the other Mn oxides. Though valence-band spectra have been measured for the MnO, Mn_3O_4, α-Mn_2O_3, and β-MnO_2 (Ref. 55) compounds, no quantitative statements about their insulating versus metallic properties are available in the literature (at least, to our knowledge). In the aforementioned HF study,[14] the authors describe Mn_3O_4 as a magnetic insulator with an electronic gap of about 10 eV. However, we want to reiterate that due to the absence of correlation, HF predictions of gaps usually overestimate the experimental values. For example, for MnO, HF gives a gap of $\approx$12 eV, three times larger than experiment.

A recent experimental study of Sato *et al.* investigated the transport properties of β-MnO_2. It was shown, in agreement with a previous work of Rogers *et al.*,[53] that the conductivity is very sensitive to the magnetic ordering. The resistivity is found to increase with decreasing temperature, reaching very large values (of the order of 10^5 Ω cm) at $T=0$ K, which indicates an insulating state. In line with these findings, the tight-binding approach of Zhuang and Halley[21] yielded an insulating ground state with a gap (in the range of 0.1 to 1.0 eV), with the size strongly dependent on the technical parameters of their approach. Also, the optimized magnetic ordering was affected by this dependency.

Results of our calculations are collected in Table IV. Each value refers to the most stable magnetic ordering as discussed in the previous section. In the absence of experimental results for Mn_3O_4, α-Mn_2O_3, and β-MnO_2, we list the experimental value for the gap only for MnO (last column). As expected, PBE provides an unsatisfactory description: (i) the gap for MnO is strongly underestimated, in agreement with previous calculations, and (ii) a metallic nature is assigned to all other compounds. Discussing the other approaches of our study, we see that the results derived from PBE+U and hybrid DFT are significantly different. Independently from the value of U, the PBE+U approach attributes an insulating character to MnO, a half-metallic (HM) state to Mn_3O_4 and α-Mn_2O_3, and a pure metallic nature to β-MnO_2. In contrast to that, PBE0 and HSE favor an insulating groundstate for all Mn oxides, though the value of the insulating gap is progressively reduced with decreasing Mn concentration, i.e. going downwards the bottom of the table. α-Mn_2O_3 does not quite follow this trend, but one needs to take into account that it is the only compound with a FM ordering in PBE0 and HSE, and a widely disparent gap for the majority and minority states. The average gap for majority and minority spin components follows this trend much better.

In agreement with previous applications of hybrid-DFT approaches, HSE yields smaller gaps than PBE0, due to the truncation of the long-range part of the Coulomb kernel in the exchange interaction, as discussed in Sec. II. The lack of experimental data does not allow for a clear conclusion concerning the quality of the predictions. Nevertheless, the metallic or partially metallic nature of Mn_3O_4, α-Mn_2O_3, and β-MnO_2 obtained by PBE and PBE+U seems inappropriate: the composition of these oxides rather suggests that they are semiconductors because of the splitting between t_{2g} and e_g levels. Within PBE and PBE+U, the crystal field splitting is not sufficient to open the gap. Furthermore, based on experimental findings one might deduct that at $T=0$, β-MnO_2 is indeed a semiconductor, as pointed out above.

The total density of states (DOS) for MnO, Mn_3O_4, α-Mn_2O_3, and β-MnO_2 using PBE, PBE+U (U=4 eV), PBE0, and HSE are compared in Figure 3. The values of the calculated gaps are also reported in each panel, and, for the insulating phases, shadowed areas mark the gap region.

For MnO, the spectra are qualitatively similar for all methods, whereas for the other oxides the applied methods yield different results. MnO is the simplest case: with an oxidation state of 2+, the remaining five Mn electrons fill the majority $3d$ states, the minority $3d$ states remain empty, and a gap arises between the filled and empty manifold regardless of the theoretical description.

In Mn_3O_4, the Mn atoms are either in the 2+ (tetrahedral) or 3+ oxidation state (octahedral). For the tetrahedral sites,

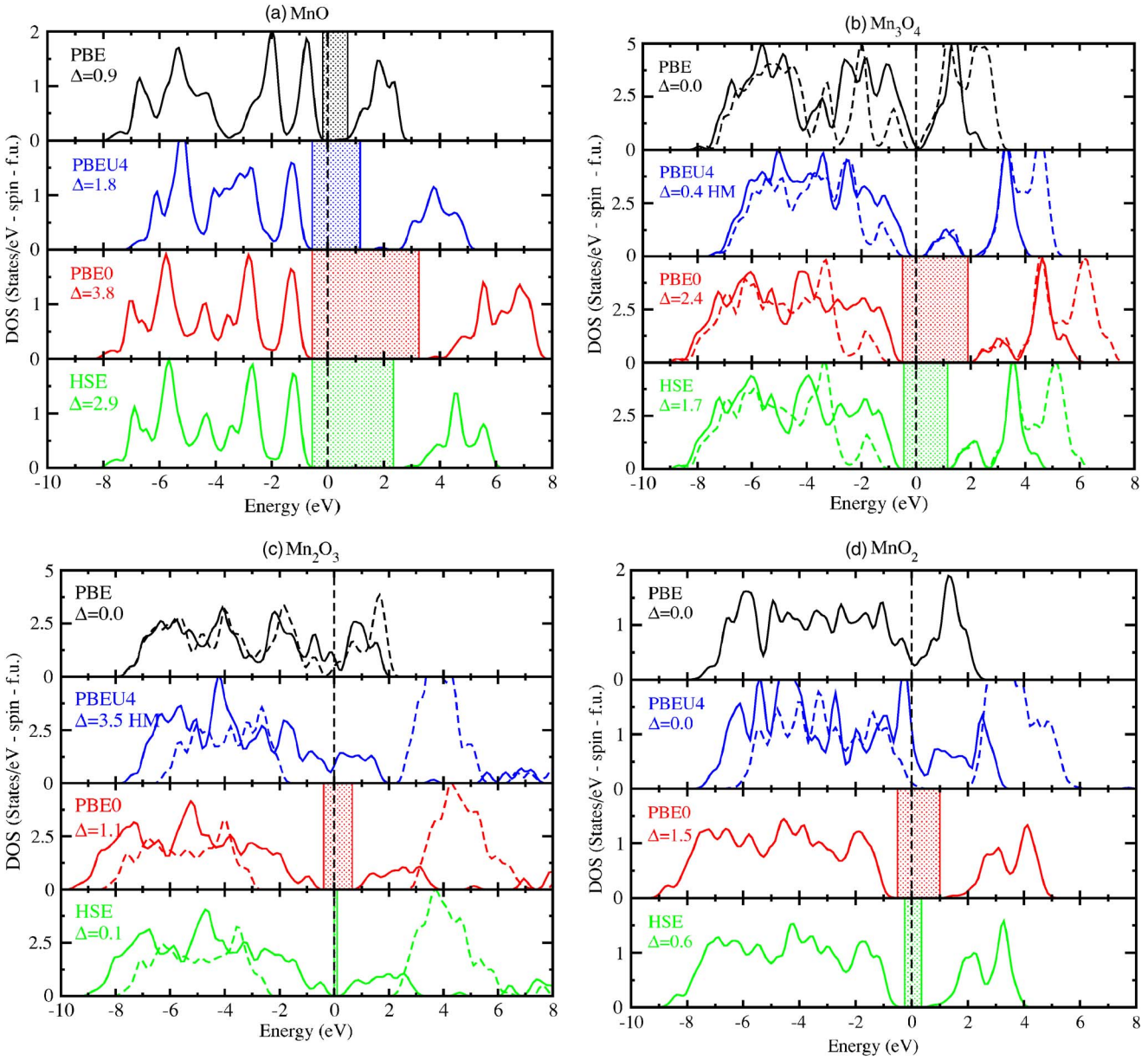

FIG. 3. (Color online) Calculated spin resolved DOS for (a) MnO, (b) Mn_3O_4, (c) α-Mn_2O_3, and (d) β-MnO_2 within PBE, PBE+U (U=4 eV), PBE0, and HSE. Shadowed areas depict the gap region.

the majority 3*d* shell is again entirely filled, whereas for *each* octahedral Mn site a *single hole* remains in the majority 3*d* shell. The minority 3*d* manifold is again essentially empty at the octahedral and tetrahedral site. Standard DFT (PBE) predicts no band gap. The PBE+U method pushes the filled majority states to lower energies, and the unoccupied minority states to higher energies, but it is not able to sufficiently separate the hole in the majority channel from the filled 3*d* states. The structure of the DOS is, however, already remarkably similar to the hybrid functionals. The orbital dependent hybrid functionals are finally able to energetically separate the hole in the majority spin channel from the remaining four filled *d* states at the octahedral site. The important technical difference between the PBE+U and the hybrid approach is that the former acts only within the PAW spheres, and this restriction does not allow the opening of a gap within the e_g shell, whereas the hybrid functionals act in the entire space and are able to separate the e_g shell into one filled and one empty e_g orbital. We believe that the HSE functional offers a very realistic description of the nonlocal screened exchange interaction in this particular case, but a definite answer about the existence of a gap requires methods beyond Kohn-Sham density functional theory (i.e. *GW*). Alternatively, a systematic calibration of the optimal amount of Fock exchange would probably shed some light on this system. However, this *semiempirical* approach would require accurate experimental data which are at present not available.

For α-Mn_2O_3 the situation is very similar as for Mn_3O_4. The description on the PBE level is most likely unrealistic, whereas the PBE+U approach yields a density of states that possess a very similar structure as the hybrid functionals. Again the formal oxidation state of Mn is 3+, implying the

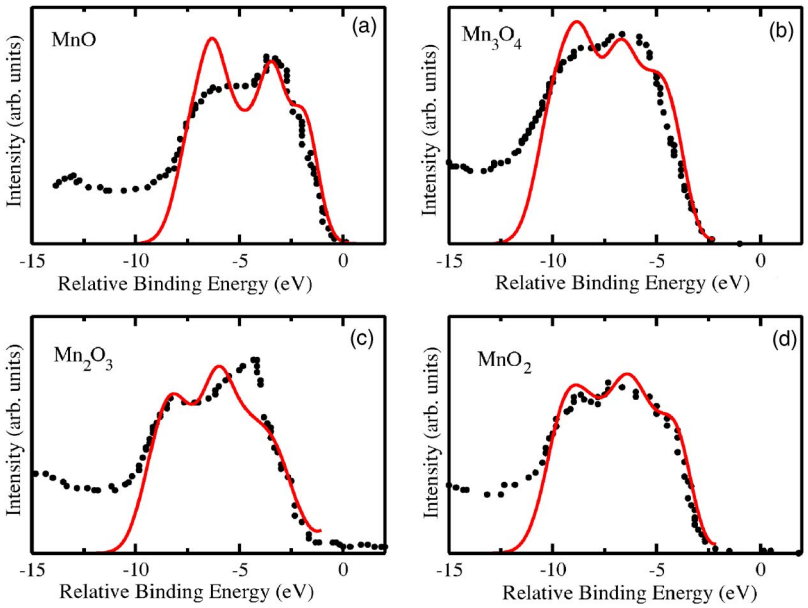

FIG. 4. (Color online) Comparison between the *d*-like DOS of the HSE calculation (full line) in comparison to the experimental XPS valence-band spectra for (a) MnO, (b) Mn_3O_4, (c) α-Mn_2O_3, and (d) β-MnO_2, according to Ref. 55. The levels of the experimental and calculated valence-band maxima are aligned. The calculated DOS is convoluted by a Gaussian with a width of σ=0.6 eV.

existence of a single hole in the majority 3*d* channel at each Mn site. PBE+U is not able to separate this hole from the filled majority states, whereas the hybrid functionals open a small band gap. The final answer whether a gap exists or not will require, again, a treatment beyond density functional theory.

In β-MnO_2 the formal oxidation state is finally 4+. The t_{2g} majority states are occupied, whereas the e_g majority states are empty. But the crystal field splitting is not sufficient to open the gap within the majority channel, and exchange and correlation effects are finally again decisive. Since these are differently treated in different methods, the answer depends on the applied functional, with the HSE method yielding a small gap, whereas the PBE+U method again fails to open the gap (note that the PBEU4 description yields a FM ground state, whereas the PBE, PBEU3, and HSE functional give an AFM ground state, see Table III). In summary, (i) PBE tends to stabilize a metallic character, although the depletion of the density of states near the Fermi energy suggests a rather low conductivity; (ii) PBE+U reinforces the half-metallic character, due to one insulating spin channel (though, for β-MnO_2 the gap is found slightly above the Fermi level, thus destroying a formal insulating character); (iii) hybrid DFT enhances the insulating character, although HSE gaps are found to be typically 1 eV smaller that the PBE0 gaps (see also Ref. 44).

Finally, Fig. 4 shows experimental x-ray photoemission spectra[55] in combination with our calculated HSE valence density of states, which are broadened by convoluting with a Gaussian. To facilitate the interpretation of the figure, the experimental and calculated valence-band maxima are aligned. The overall agreement between experiment and calculations is rather satisfactory. The width of the valence band is well reproduced, as well as the slope of the topmost part, and, furthermore, the saddle-point structure right below the band maxima. The calculated structures of the peaks, though less precisely reproduced, are still in good agreement with the measured data.

D. Energy of formation

The energy of formation ΔH, at T=0 K is defined by

$$\Delta H = E^{\mathrm{Mn}_x\mathrm{O}_y} - xE^{\gamma\text{-Mn}} - y\tfrac{1}{2}E^{\mathrm{O}_2}, \tag{1}$$

in which $E^{\mathrm{Mn}_x\mathrm{O}_y}$, $E^{\gamma\text{-Mn}}$, and E^{O_2} are the DFT total energies for the given oxide, the γ phase of bulk Mn, and the oxygen molecule O_2, respectively. The subscripts x and y denote the manganese and oxygen composition. Two assumptions are made: (i) the zero-point vibrations are neglected, and (ii) the γ phase of pure Mn was chosen as reference, because the α phase, being the low temperature ground state, requires demanding calculations due to its complex geometrical and magnetic structure. Assumption (ii) is justified, because—as published by Hafner and Hobbs[58]—the energy difference between these two phases is only 0.67 meV within a standard DFT approach. We have treated the O_2 molecule in an orthorhombic box with a cutoff of 1000 eV, including aspherical corrections.

The calculated energies of formation are summarized in Table V and compared with available experimental data (a pictorial view is given by Fig. 5). The absolute relative error with respect to the measured energies is also given. First, we point out that the PBE functional underestimates the energies of formation. As expected, the relative error is larger for higher correlated system such as MnO (RE=35%) than for β-MnO_2 (RE=11%), for which the limitations of PBE in treating the exchange and correlation contributions are less pronounced.

Much better results are achieved using hybrid functionals and PBE+U. Both yield remarkably similar results, at least for U=3 and U=4. The underbinding is drastically reduced, in particular, in the reduced Mn rich compounds. This is most likely related to a significant destabilization of the Mn metal using the hybrid and PBE+U functional. It is certainly interesting why the results for the formation energies using HSE and PBE+U are so similar, and we will return to this issue in the summary and conclusions.

TABLE V. Calculated energy of formation ΔH (eV) compared to the experimental measurements taken from Ref. 57. The corresponding relative error (RE) are mean absolute relative error (MARE) are also reported.

	PBEU6	PBEU4	PBEU3	PBE	PBE0	HSE	Expt.
MnO	−4.043	−3.932	−3.798	−2.583	−3.826	−3.826	−3.989
	−1	1	5	35	4	4	
Mn_3O_4	−12.944	−13.677	−13.400	−11.145	−13.549	−13.784	−14.378
	10	5	7	22	6	4	
α-Mn_2O_3	−8.667	−9.386	−9.279	−8.051	−9.212	−9.033	−9.935
	13	6	7	19	7	9	
β-MnO_2	−3.762	−4.512	−4.631	−4.783	−4.422	−4.468	−5.387
	30	16	14	11	18	17	
MARE	14	7	8	22	9	9	

Concerning the *relative formation energies*, which are important to determine at which chemical potential the reaction $Mn_xO_y \rightarrow Mn_xO_{y-1} + 1/2O_2$ takes place, we observe that the PBE functional gives a completely different trend than the hybrid (and PBE+U) functional. Standard DFT (PBE) favors oxygen-rich compounds (largest underbinding for MnO), whereas HSE, PBE0, and PBE+U incorrectly favor oxygen-poor compounds (largest underbinding for MnO_2). The situation is obviously not satisfactory in any of the descriptions. It is difficult to tell whether the error is related to an inadequate description of the O_2 molecule or an inadequate description of exchange and correlation in the compounds themselves, but from a pragmatic point of view, the agreement with experiment can be improved by destabilizing the O_2 molecule by 0.3 eV per 1/2 O_2. The MARE for the PBE+U case then reduces to 4%, whereas that for the hybrid functionals reduces to 7–8 %. Recently Wang *et al.*[32] made a similar observation for a wide class of (transition) metal oxides using the PBE+U method, and suggested that the O_2 molecule is overbound by roughly 0.6 eV per 1/2 O_2 in the PBE functional. Although we prefer to phrase the statement more cautiously—i.e., PBE overestimates the oxygen binding energy in O_2 compared to many metal oxides by roughly 1/2 eV—our present calculations overall seem to confirm their conjecture. To make that point clear, we cannot tell whether the error is related to deficiencies in the description of O_2 (for instance, large surface effects), or in the description of correlation effects in the transition-metal oxides. The last point is, for instance, supported by the observation that in the oxygen-rich reduce regime (MnO_2), gaps are small and electronic screening might be rather strong, and an adequate description might require less than 1/4 of the nonlocal Fock exchange. Obviously, no mean-field approach with a fixed amount of nonlocal exchange will ever be able to describe redox reactions entirely adequately.

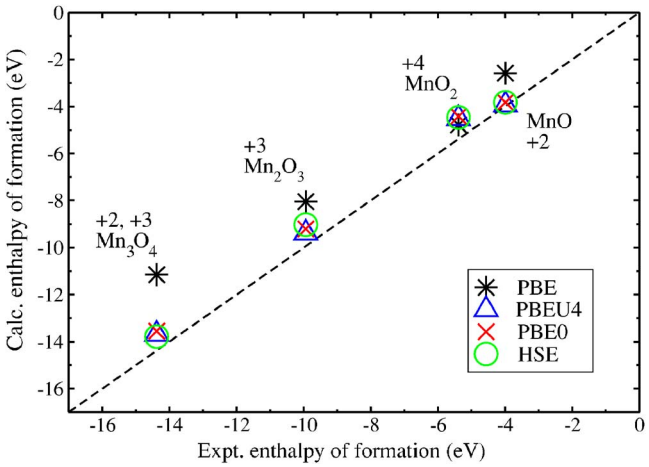

FIG. 5. (Color online) Comparison of calculated and experimental energies of formation (eV). The numerical labels indicate the oxidation state.

IV. SUMMARY AND CONCLUSIONS

We have presented a comprehensive study of the ground-state properties of MnO, Mn_3O_4, α-Mn_2O_3, and β-MnO_2, using four different methods to treat exchange and correlation, namely standard PBE, PBE+U and hybrid functionals, PBE0, and HSE. All approaches have been applied consistently within the same PAW-DFT framework, as implemented in the VASP package.

The lack of accurate experimental informations on the electronic properties and the difficulties encountered in dealing with unusually complicated magnetic orderings makes it difficult to judge which is the most appropriate. However, on the basis of the results discussed in the previous sections, we conclude that hybrid functionals appear to provide the most balanced and consistent description, as argued below.

(i) PBE0 and HSE yield equilibrium volumes within 1% of the experimental values, in contrast to PBE+U which suffers from a large volume overestimation, leading to deviations from experiment of about 4–7 %. Standard PBE provides equilibrium volumes in good agreement with experiment, but it fails in giving reasonable electronic properties: the PBE approach favors a metallic character for all studied oxides, with the exception of MnO, whose band gap, however, turns out to be far too small. Finally, PBE underestimates the energy of formations by more than 20%.

(ii) PBE+U accounts relatively well for the calculated

energies of formation. In agreement with previous studies,[32] we find that U=4 eV yields the best energy of formations, as compared to experiment. However, this choice is a practical compromise to overcome the limitations of DFT+U methods, for which total energies referring to different values of U cannot be compared. In fact, there are no rigorous arguments which justify the choice of the same U for different manganese oxides with quite different exchange and correlation interactions. It is remarkable that a U of 3–4 eV is roughly a quarter of the unscreened Coloumb repulsion U in the free atom. In this sense, a U of 3–4 eV is consistent with the choice made in the PBE0 and HSE03 functional: i.e., one quarter of the nonlocal Fock exchange. The difference between both approaches is then entirely in the way these nonlocal exchange and correlation effects are accounted for. In the LDA+U method, the improved treatment of the correlation effects is limited to states localized inside the atomic spheres, essentially the Mn 3*d* states, whereas the hybrid functionals use an orbital dependent functional operating on all states, extended as well as localized. The treatment of exchange and correlation effects within the O 2*p* band is automatically improved only by the latter method. Apart from that it is obvious that the amount of nonlocal exchange and the U parameter are system dependent.[27–30] Exchange dominated systems with large band gaps (MnO in the present case) "require" more exact exchange, whereas MnO_2, which approaches the metallic regime, is not exchange dominated, and a proper description might require less than one quarter of the exact exchange or a smaller U.[29,31] This might be the main reason why the energies of MnO_2 are not well described. The only mean-field theory capable of seamlessly uniting these two extremes is the *GW* method, but the complex systems investigated here are presently hardly accessible using the *GW* method.[58]

(iii) Summarizing the results for the electronic structure, we remark that the one-particle Kohn-Sham DOS cannot be directly compared to measured spectra. Therefore, the discussion of band gaps needs some caution. Limiting ourselves to a qualitative understanding, we find that although PBE+U and hybrid DFT provide a different metallic/insulating chracter for Mn_3O_4, α-Mn_2O_3, and β-MnO_2, the density of states are rather similar both in shape and width. Considering that the existence of a gap cannot be unambiguously ascertained with any of the present methods for the reasons given above, a critical judgment on the performance of PBE+U and hybrid DFT functionals cannot be made. To improve the present understanding of the ground-state properties of manganese oxides and to confirm the apparent insulating regime of Mn_3O_4, α-Mn_2O_3, and β-MnO_2 at low temperatures, more detailed and accurate experimental data are urgently required.

ACKNOWLEDGMENTS

Financial support by the Austrian Science Fund FWF within the Joint Research Program S90, and the START project Y218 is gratefully acknowledged.

*Also at SLACS, Sardinian Laboratory for Computational Materials Science, University of Cagliari, Italy.

[1] J. E. Post, PNAS **96**, 3447 (1999).
[2] R. N. Iskenderov, I. A. Drabkin, L. T. Emel'yanova, and Ya. M. Ksendzov, Fiz. Tverd. Tela (Leningrad) **10**, 2573 (1968) [Sov. Phys. Solid State **10**, 2031 (1969)].
[3] B. E. F. Fender, A. J. Jacobson, and F. A. Wegwood, J. Chem. Phys. **48**, 990 (1968).
[4] H. Shaked, J. Faber, Jr., and R. L. Hitterman, Phys. Rev. B **38**, 11901 (1988).
[5] S. Massidda, A. Continenza, M. Posternak, and A. Baldereschi, Phys. Rev. Lett. **74**, 2323 (1995).
[6] A. Filippetti and N. A. Spaldin, Phys. Rev. B **67**, 125109 (2003).
[7] M. Posternak, A. Baldereschi, S. Massidda, and N. Marzari, Phys. Rev. B **65**, 184422 (2002).
[8] X. B. Feng, Phys. Rev. B **69**, 155107 (2004).
[9] C. Franchini, V. Bayer, R. Podloucky, J. Paier, and G. Kresse, Phys. Rev. B **72**, 045132 (2005).
[10] V. Bayer, C. Franchini, and R. Podloucky, Phys. Rev. B **75**, 035404 (2007).
[11] K. Dwight and N. Menyuk, Phys. Rev. **119**, 1470 (1960).
[12] G. Srinivasan and M. S. Seehra, Phys. Rev. **28**, 1 (1926).
[13] B. Chardon and F. Vigneron, J. Magn. Magn. Mater. **58**, 128 (1986).
[14] A. Chartier, P. D'Arco, R. Dovesi, and V. R. Saunders, Phys. Rev. B **60**, 14042 (1999).
[15] R. W. Grant, S. Geller, J. A. Cape, and G. P. Espinosa, Phys. Rev. **175**, 686 (1968).
[16] S. Mukherjee, A. K. Pal, S. Bhattacharya, and J. Raittila, Phys. Rev. B **74**, 104413 (2006).
[17] M. Regulski, R. Przenioslo, I. Sosnowska, D. Hohlwein, and R. Schneider, J. Alloys Compd. **362**, 236 (2004).
[18] M. Regulski, R. Przenioslo, I. Sosnowska and J. U. Hoffmann, Phys. Rev. B **68**, 172401 (2003).
[19] H. Sato, T. Enoki, M. Isobe, and Y. Ueda, Phys. Rev. B **61**, 3563 (2000).
[20] A. Yoshimori, J. Phys. Soc. Jpn. **14**, 807 (1959).
[21] M. Zhuang and J. W. Halley, Phys. Rev. B **64**, 024413 (2001).
[22] R. O. Jones and O. Gunnarsson, Rev. Mod. Phys. **61**, 689 (1989).
[23] V. I. Anisimov, J. Zaanen, and O. K. Andersen, Phys. Rev. B **44**, 943 (1991).
[24] A. Svane and O. Gunnarsson, Phys. Rev. Lett. **65**, 1148 (1990).
[25] L. Hedin, Phys. Rev. **139**, A796 (1965).
[26] A. D. Becke, J. Chem. Phys. **98**, 1372 (1993).
[27] D. Muñoz, N. M. Harrison, and F. Illas, Phys. Rev. B **69**, 085115 (2004).
[28] X. Feng and N. M. Harrison, Phys. Rev. B **70**, 092402 (2004).
[29] M. Alfredsson, G. D. Price, C. R. A. Catlow, S. C. Parker, R. Orlando, and J. P. Brodholt, Phys. Rev. B **70**, 165111 (2004).
[30] I. Ciofini, F. Illas, and. C. Adamo, J. Chem. Phys. **120**, 3811 (2004).
[31] I. P. R. Moreira, F. Illas, and R. L. Martin, Phys. Rev. B **65**,

155102 (2002).
[32] L. Wang, T. Maxisch, and G. Ceder, Phys. Rev. B **73**, 195107 (2006).
[33] J. P. Perdew, M. Ernzerhof, and A. Bruke, J. Chem. Phys. **105**, 9982 (1996).
[34] P. E. Blöchl, Phys. Rev. B **50**, 17953 (1994).
[35] G. Kresse and D. Joubert, Phys. Rev. B **59**, 1758 (1999).
[36] G. Kresse and J. Hafner, Phys. Rev. B **48**, 13115 (1993).
[37] G. Kresse and J. Furthmüller, Comput. Mater. Sci. **6**, 15 (1996).
[38] J. P. Perdew, K. Burke, and M. Ernzerhof, Phys. Rev. Lett. **77**, 3865 (1996).
[39] S. L. Dudarev, G. A. Botton, S. Y. Savrasov, C. J. Humphreys, and A. P. Sutton, Phys. Rev. B **57**, 1505 (1998).
[40] M. Ernzerhof and G. E. Scuseria, J. Chem. Phys. **110**, 5029 (1999).
[41] J. Heyd, G. E. Scuseria, and M. Ernzerhof, J. Chem. Phys. **118**, 8207 (2003).
[42] J. Heyd and G. E. Scuseria, J. Chem. Phys. **120**, 7274 (2004).
[43] J. Paier, R. Hirschl, M. Marsman, and G. Kresse, J. Chem. Phys. **122**, 234102 (2005).
[44] J. Paier, M. Marsman, K. Hummer, G. Kresse, I. C. Gerber, and J. G. Ángyán, J. Chem. Phys. **124**, 154709 (2006).
[45] J. Heyd, G. E. Scuseria, and M. Ernzerhof, J. Chem. Phys. **124**, 219906 (2006).
[46] H. J. Monkhorst and J. D. Pack, Phys. Rev. B **13**, 5188 (1976).
[47] W. B. Pearson, *A Handbook of Lattice Spacings, and Structures of Metals and Alloys* (Pergamon, Ney York, 1958).
[48] W. G. Wykoff, *Crystal Structures* (Wiley, New York, 1963).
[49] S. Geller, Acta Crystallogr., Sect. B: Struct. Crystallogr. Cryst. Chem. **27**, 821 (1971).
[50] N. Ohama and Y. Hamaguchi, J. Phys. Soc. Jpn. **30**, 1311 (1971).
[51] B. E. F. Fender, A. J. Jacobson, and F. A. Wegwood, J. Chem. Phys. **48**, 990 (1968).
[52] A. K. Cheetham and D. A. O. Hope, Phys. Rev. B **27**, 6964 (1983).
[53] D. B. Rogers, R. D. Shannon, A. W. Sleight, and J. L. Gillson, Inorg. Chem. **8**, 841 (1969).
[54] R. N. Iskenderov, I. A. Drabkin, L. T. Emel'yanova, and Y. M. Ksendzov, Fiz. Tverd. Tela (Leningrad) **10**, 2573 (1968) [Sov. Phys. Solid State **10**, 2031 (1969)].
[55] A. A. Audi and P. M. A. Scherwood, Surf. Interface Anal. **33**, 274 (2002).
[56] I. A. Drabkin, L. T. Emel'yanova, R. N. Iskenderov, and Y. M. Ksendzov, Fiz. Tverd. Tela (Leningrad) **10**, 3082 (1968) [Sov. Phys. Solid State **10**, 2428 (1969)].
[57] S. Fritsch and A. Navrotsky, J. Am. Chem. Soc. **79**, 1761 (1996).
[58] J. Hafner and D. Hobbs, Phys. Rev. B **68**, 014408 (2003).